Dalton Transactions

Rhenium bipyridine catalysts with hydrogen bonding pendant amines for CO2 reduction

Journal:	*Dalton Transactions*
Manuscript ID	DT-COM-06-2019-002689.R1
Article Type:	Communication
Date Submitted by the Author:	22-Aug-2019
Complete List of Authors:	Hellman, Ashley; University of Southern California, Chemistry Haiges, Ralf; University of Southern California, Chemistry Marinescu, Smaranda ; University of Southern California, Chemistry

COMMUNICATION

Rhenium bipyridine catalysts with hydrogen bonding pendant amines for CO_2 reduction

Received 00th January 20xx,
Accepted 00th January 20xx

DOI: 10.1039/x0xx00000x

Ashley N. Hellman, Ralf Haiges and Smaranda C. Marinescu*

ABSTRACT: Rhenium tricarbonyl bipyridine complexes modified with pendant secondary and tertiary amines in the 6- and 6'-positions were synthesized and characterized. Electrocatalytic studies performed under CO_2 with 2,2,2,-trifluoroethanol display large current densities, corresponding to the reduction of CO_2 to CO with moderate Faradaic efficiencies (51-73%).

The electrochemical conversion of CO_2 to valuable chemicals and fuels is an important step toward creating a carbon-neutral infrastructure.[1] In nature, the enzyme CO-dehydrogenase (CODH) catalyzes the selective conversion of CO_2 to CO with high activity.[2–4] The CO_2 activation is facilitated by hydrogen bonding interactions between the bound substrate and the amino acid residues present in the secondary coordination sphere.[2–4] Due to the high thermodynamic barrier associated with the reduction of CO_2 to CO, a catalyst capable of reducing CO_2 via proton-coupled electron transfer (PCET) steps is attractive for lowering the required energy.[5–7] A variety of bio-inspired CO_2-reduction electrocatalysts with pendant proton donors have been reported, such as nickel cyclams with pendant amines[8–10], iron porphyrins with pendant phenolic,[11] trimethylanilinium,[12] and amide[13] groups, and cobalt aminopyridine macrocycles with pendant amines.[14,15]

Metal bipyridine complexes, including $Re(bpy)(CO)_3Cl$ and $Mn(bpy)(CO)_3Cl$ (bpy = 2,2'-bipyridine), are some of the most well-studied classes of electrocatalysts for CO_2 reduction.[16–19] In particular, $Re(bpy)(CO)_3Cl$ has been shown to have good selectivity for the reduction of CO_2 to CO, although with low catalytic rate constants and deactivation via dimerization. However, the performance of Mn and Re bipyridine catalysts can be modulated through the addition of pendant groups capable of hydrogen bonding interactions. Manganese bipyridine complexes modified with pendant phenolic,[20] methoxy,[21] and imidazolium[22] groups exhibit increased current enhancements at more positive potentials than $Mn(bpy)(CO)_3Cl$. We have previously reported that a rhenium bipyridine catalyst modified with pendant amines in the 5- and 5'-positions converts CO_2 to CO with a 99% Faradaic efficiency (FE), although at more negative potentials than that of other reported rhenium bipyridine catalysts.[23] Bio-inspired rhenium bipyridine catalysts modified with amino acid substituents in the 4- and 4'-positions undergo both inter- and intramolecular hydrogen bonding interactions, leading to current increases at approximately 250 mV more positive potentials than that of $Re(bpy)(CO)_3Cl$, due to the promotion of an alternative bimolecular mechanism.[24] Rhenium bipyridine complexes bearing di- and tri-phenolic groups display current enhancements at both the first and second reduction potentials under CO_2 with added H_2O, but undergo electrode passivation during catalysis, yielding turnover numbers (TON) between 2 and 14.[25] An aminophenethyl-modified rhenium bipyridine catalyst exhibits a current increase near the second reduction potential under CO_2, with near unity FE and selectivity for CO production and a TON of 6.[26] Additionally, a rhenium bipyridine complex featuring an imidazolium group shows current increases under CO_2 at a potential 170 mV more positive than that of $Re(bpy)(CO)_3Cl$.[27] This increased activity was attributed to hydrogen bonding second-sphere interactions present in the imidazolium catalyst.[27] Motivated by the prior work on bio-inspired rhenium bipyridine catalysts, we report here a family of substituted rhenium bipyridine catalysts with pendant secondary and tertiary amines and explore their electrochemistry for CO_2 reduction.

Amine-substituted bipyridine ligands **L^1–L^4** were synthesized using a modified Ullmann coupling procedure (Scheme 1 and S1). Ligands **L^1** and **L^2** display a broad resonance at δ 4.55 and 4.58 ppm, respectively, corresponding to the N*H* moieties (Figures S1–S4). Rhenium complexes **1–4** were generated by refluxing **L^1–L^4** with $Re(CO)_5Cl$ in anhydrous toluene for 12 h. The ^{1}H NMR resonances of complexes **1–4** are shifted downfield in comparison to the corresponding resonances of ligands **L^1–L^4**, as expected upon addition of the electron withdrawing rhenium metal center (Figures S5–S8). Complexes **1** and **2** each display a broad resonance at δ 6.23 and 6.09 ppm, respectively, corresponding to the N*H* moieties.

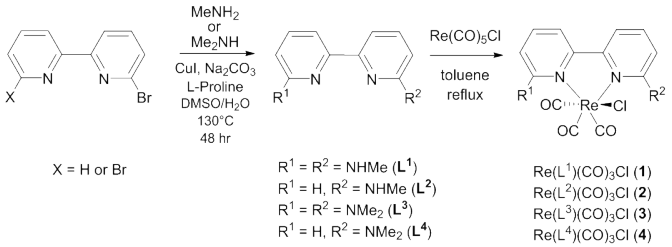

[a] *Department of Chemistry, University of Southern California, Los Angeles, CA 90089, United States of America. E-mail: smarines@usc.edu.*

†Electronic Supplementary Information (ESI) available: Detailed experimental procedures, characterization including spectroscopic, diffraction, and electrochemical data. CCDC 1908117-1908120. See DOI: 10.1039/x0xx00000x

Scheme 1. Synthetic scheme for complexes **1–4**.

Single crystal X-ray diffraction studies of complexes **1–4** reveal equatorial coordination of the bipyridine ligand and a facial arrangement of the three carbonyl moieties, typical of other Re(bpy)$(CO)_3$ complexes (Figure 1 and S9). Due to low quality diffraction data for complex **3**, bond lengths and angles will only be discussed for complexes **1**, **2**, and **4**. The Re–N(pyridine) bond lengths in complexes **1** and **2** range between 2.18 and 2.20 Å, and are analogous to those observed for the Re(bpy)$(CO)_3$Cl (2.17 Å).[28] However, the Re–N bond lengths in complex **4** are de-symmetrized: one is slightly shorter (2.162(2) Å), and one is elongated to 2.226(2) Å, due to the presence of the bulky dimethylamino group. Further, while the bipyridine ligand in complexes **1** and **2** are essentially planar, with bipyridine N—C—C—N torsion angles of only 0.6(3)° and 1.3(3)°, respectively, complex **4** has a torsion angle of 12.2(2)° (Figures S10-S11).

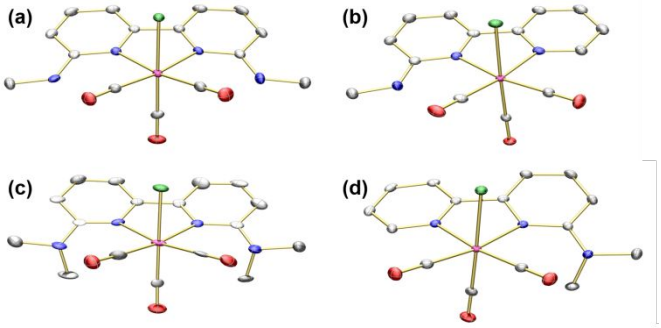

Figure 1. Solid state structures of (a) **1**, (b) **2**, (c) **3**, and (d) **4**. Color legend of the atoms: gray – C; blue – N; red – O; green – Cl; pink – Re. Solvent molecules and hydrogen atoms are excluded for clarity.

Complexes **1–4** were further characterized by FT-IR spectroscopy. Three carbonyl stretches are observed for each complex: one high-energy mode (a_1') and two lower-energy modes (a" and a_2'), as expected for *fac*-Re$(CO)_3$ complexes (Figures S12-S15 and Table S1).[29,30] The a_1' mode displays a slight red-shift from 2011 to 2013 cm^{-1} in complexes **1** and **3**, respectively, and from 2014 to 2016 cm^{-1} in complexes **2** and **4**, respectively, as expected upon increasing the electron density of the bipyridine substituents. This difference, although minimal, indicates a slightly greater electron density at the rhenium center for the bis-substituted complexes compared to the mono-substituted complexes. Complexes **1** and **2** also display bands at 3416 and 3391 cm^{-1}, respectively, corresponding to the N-H stretches (Table S1).

Cyclic voltammetry (CV) experiments of complexes **1–4** under N_2 display either a reversible or quasi-reversible first reduction feature followed by an irreversible second reduction feature (Figures 2 and S16-S19). All potentials are listed versus $Fc^{+/0}$. Complexes **1** and **3** exhibit the first reduction feature at -1.96 V and -1.92 V, respectively, and the second reduction feature at -2.25 V and -2.26 V, respectively (Table S2). Complexes **2** and **4** display the first reduction feature at -1.87 V and -1.84 V, respectively, and the second reduction feature at -2.16 V and -2.19 V, respectively. The reduction potentials of complexes **1** and **3** are slightly more negative in comparison to those of complexes **2** and **4** due to an increased number of electron donating groups (NMe). All four complexes display reduction features at more negative potentials than the unsubstituted complex, Re(bpy)$(CO)_3$Cl, which has reduction features at -1.75 V and -2.12 V under identical conditions. Randles-Sevcik plots indicate that complexes **1–4** are all freely diffusing in solution (Figures S20-S23).

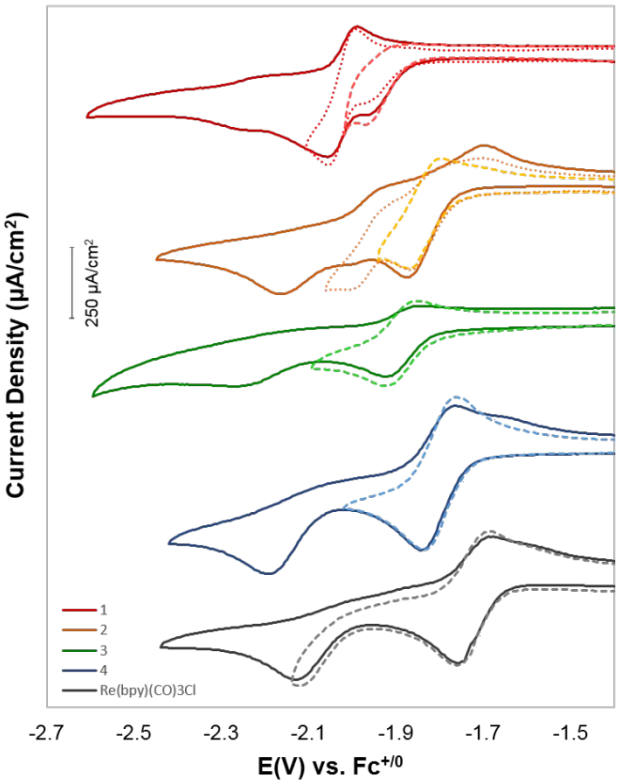

Figure 2: CVs of 1 mM **1** (red), **2** (orange), **3** (green), **4** (blue), and Re(bpy)$(CO)_3$Cl (gray) under N_2 in a 0.1 M $TBAPF_6$ MeCN solution. Dashed lines illustrate the first reduction feature, and dotted lines (**1** and **2**) show the presence of an additional intermediate reduction feature. Scan rate: 100 mV/s.

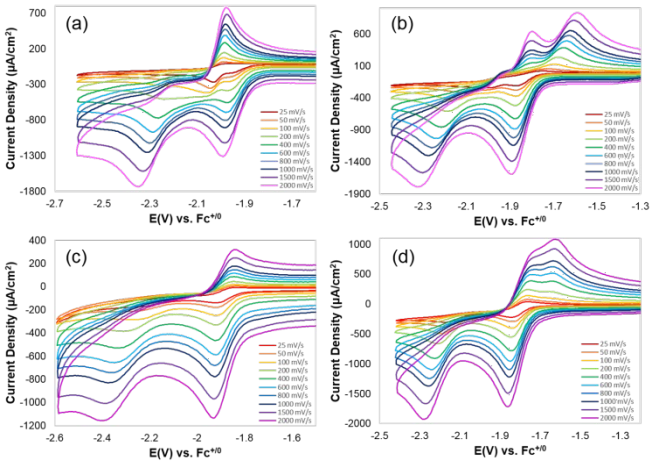

Figure 3: Variable scan rate studies of (a) **1**, (b) **2**, (c) **3**, and (d) **4**. Conditions: 1 mM catalyst in MeCN with 0.1 M $TBAPF_6$.

Complexes **1** and **2** both exhibit an additional reduction feature at -2.05 and -2.01 V, respectively, at 100 mV/s (Figure 2). Variable scan rate studies of complexes **1** and **2** show that this additional reduction feature disappears at faster scan rates (above 400 mV/s), suggesting that this reduction event is coupled to a chemical process which proceeds too slowly to be observed on the CV timescale (Figure 3). This chemical process is assigned to Re—Re

dimerization, which has been reported previously in analogous rhenium bipyridine catalysts.[31] In contrast, complexes **3** and **4**, which lack NH moieties, do not display this additional feature even at low scan rates. This behavior suggests that dimerization is facilitated by the presence of pendant NH moieties, which may engage in hydrogen bonding interactions. Because MeCN is a poor hydrogen bond donor and acceptor, the solute—solute hydrogen bonding interactions that facilitate Re—Re dimerization are expected to be more prevalent in MeCN than in DMF.[32] To further probe the proposed hydrogen bonding interactions, the electrochemistry of **2** was explored in DMF. CVs of **2** in DMF under N_2 exhibit reduction features at -1.91 and -2.28 V, consistent with the two reduction features typically observed for rhenium bipyridine complexes (Figure S68). A third irreversible feature at -2.45 V is observed and assigned to the dimerization. Interestingly, this reduction appears at a potential more negative than the additional feature in MeCN, suggesting that DMF can disrupt the hydrogen bonding interactions and reduce the extent of hydrogen bonding-facilitated dimerization.

Upon switching the gas from N_2 to CO_2 (1 atm), complexes **1–4** exhibit current enhancements at either the same or more negative potentials than their second reduction features (Figures S24-S28). Bis-substituted complexes **1** and **3** exhibit smaller current increases under CO_2 than mono-substituted complexes **2** and **4**. Notably, complex **4** displays a drastic increase in current under CO_2 saturation, reaching 9 mA/cm^2. Additionally, complexes **3** and **4** display trace crossing of the forward and reverse scans, indicating substrate depletion in the diffusion layer on the CV timescale (Figures S27 and S37).[33,34]

The current response upon addition of a Brønsted acid (water, methanol, 2,2,2-trifluoroethanol, or phenol) was analyzed for each complex (Figures S29-S44). While titrations with water or methanol (MeOH) led to current increases near the potentials of the second reduction features, addition of 2,2,2-trifluoroethanol (TFE) or phenol (PhOH) caused substantial current enhancements at potentials near the first reduction features. Moreover, TFE provided slightly greater current responses than PhOH, so this was chosen as the optimal acid source for further studies (Figure 4). CVs performed in the presence of TFE under N_2 show only minimal increases in current densities, indicating that the observed current responses are not due to proton reduction (Figures S45-S48).

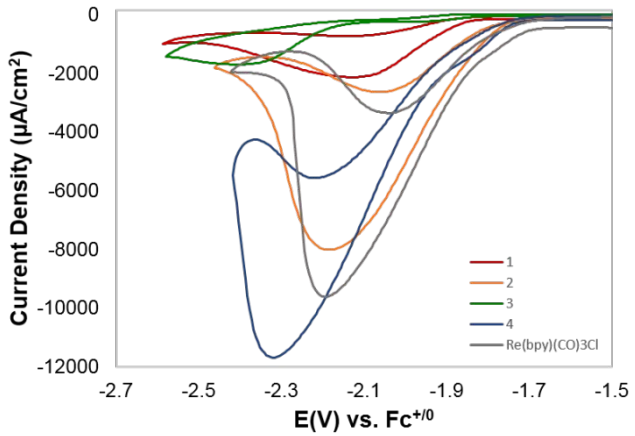

Figure 4: CVs of 1 mM **1** (red), **2** (orange), **3** (green), **4** (blue), and Re(bpy)(CO)$_3$Cl (gray) under 1 atm of CO_2 in MeCN with 0.1 M $TBAPF_6$ and TFE (2 M for complexes **1**, **2**, **4**, and Re(bpy)(CO)$_3$Cl and 0.8 M for complex **3**). Scan rate: 100 mV/s.

	E_{cat} (V vs. $Fc^{+/0}$)	FE_{CO} (%)	μmol CO	TON	i_{cat}/i_p (100 mV/s)
1	-2.10	51	55	1.4	8.2
2	-2.06	73	157	3.9	18.3
3	-2.32	53	27	0.7	22.3
4	-2.32	58	190	4.8	29.5
Re(bpy)(CO)$_3$Cl	-2.20	86	183	4.6	29.1

Table 1. Catalytic parameters for complexes **1–4** and Re(bpy)(CO)$_3$Cl (1 mM) under CO_2 in MeCN with 0.1 M $TBAPF_6$ and TFE (2 M for complexes **1**, **2**, **4**, and Re(bpy)(CO)$_3$Cl and 0.8 M for complex **3**).

Controlled potential electrolysis (CPE) experiments were performed for 1 hour under CO_2 at the potentials of maximum current density for complexes **1–4** (Figure S57). Gas chromatography (GC) analyses of the electrolysis cell headspace confirmed production of CO for complexes **1–4** (Table 1). CPE experiments with mono-substituted complexes **2** and **4** performed at -2.06 and -2.32 V produced 157 and 190 μmol CO with Faradaic Efficiencies (FE) of 73 and 58%, respectively. The amounts of CO produced by complexes **2** and **4** are comparable to that of Re(bpy)(CO)$_3$Cl (183 μmol CO and 86% FE at -2.20 V) under identical conditions. However, complex **2** attains these values at a slightly more positive potential (-2.06 V) than complex **4** and Re(bpy)(CO)$_3$Cl (-2.32 and -2.20 V, respectively). CPE experiments with bis-substituted complexes **1** and **3** at -2.10 and -2.32 V produce lower amounts of CO (55 and 27 μmol CO) with 51 and 53% FE, respectively. No other products, such as hydrogen or formic acid, were detected for any of these catalysts, and wash tests indicate that no species active for CO_2 reduction deposit on the electrode during CPE. TON were calculated for complexes **1–4** and Re(bpy)(CO)$_3$Cl according to Eq. S1. Although the values are low, all catalysts except complex **3** produce greater than one equivalent of CO per mole of catalyst in the electrolysis solution (Table 1). Electrolyses of complexes **1–4** and TFE under N_2 display low current densities and no CO production. Additionally, UV-vis spectra taken before and after electrolysis under CO_2 support retention of the original structures, suggesting that decomposition and loss of carbonyl ligands is not a contributing factor toward the production of CO (Figures S73-S74).

In the absence of TFE as an acid source, only complex **4** produced CO (44 μmol with a FE of 18%), and no other products were detected for any of the catalysts (Figure S66). Use of PhOH as the Brønsted acid for complex **2** led to steady current decreases and no formation of CO_2 reduction products (Figures S60-S61). Further, use of DMF as the solvent with TFE as the acid source for complex **2** led to a stable current response during CPE and a FE for CO analogous to that with MeCN as the solvent (71%), with 134 μmol CO produced (Figure S71-S72). CPE experiments performed in the absence of the catalysts display negligible current responses and CO production, indicating that the glassy carbon working electrode is not responsible for the observed current responses during catalysis.

As CPE studies confirmed the reduction of CO_2 to CO by complexes **1–4**, CV data recorded with added TFE were used to determine their normalized peak current values (i_{cat}/i_p, where i_{cat} = the peak current density under catalytic conditions, and i_p = the peak current density of the catalysts under N_2). These i_{cat}/i_p values were used to estimate the activity of the rhenium catalysts. Complexes **1–4** display normalized peak current values of 8.2, 18.3,

22.3, and 29.5, respectively (Table 1). The i_{cat}/i_p and value for complex **4** is comparable to that of Re(bpy)$(CO)_3$Cl (29.1) under identical conditions, suggesting similar catalytic activity. However, the calculated i_{cat}/i_p values are overall lower than those reported for other substituted rhenium bipyridine catalysts,[30] suggesting that these complexes undergo slower catalysis.

In summary, a series of rhenium bipyridine complexes modified in the 6- and 6'- positions with secondary and tertiary amines were synthesized and characterized by ^{1}H NMR, FT-IR, and single crystal X-ray diffraction. Single crystal X-ray diffraction studies of complexes **1–4** confirm the facial arrangement of the three carbonyl moieties, typical of other Re(bpy)$(CO)_3$ complexes. Cyclic voltammograms under N_2 display an additional reduction feature at slow scan rates for complexes **1** and **2**, which contain NH moieties. These additional features were attributed to hydrogen-bonding dimerization due to their disappearance in DMF. Under CO_2, complexes **1—4** display irreversible current enhancements at the second reduction feature. Titrations with TFE lead to greater current enhancements at the first reduction feature, attaining current densities up to 12 mA/cm^2 for complex **4**. During CPE experiments, mono-substituted complexes **2** and **4** performed analogously to Re(bpy)$(CO)_3$Cl under identical conditions, producing similar volumes of CO, whereas bis-substituted complexes **1** and **3** produced only small amounts of CO. Under optimized conditions, the Faradaic efficiencies for all four complexes were moderate, ranging from 51 to 73% CO produced, with no other quantifiable products observed.

This work was supported by the National Science Foundation (NSF) through the CAREER award (CHE-1555387), and by the University of Southern California (USC) and the USC Women in Science and Engineering (WiSE) program through start-up funds. We also thank the NSF (grant CRIF 1048807) and USC for their sponsorship of the NMR spectrometers and the X-ray diffractometer.

Conflicts of interest

There are no conflicts to declare.

Notes and references

1 M. E. Dry, *Catal. Today*, 2002, **71**, 227–241.
2 W. Lubitz, H. Ogata, O. Rü and E. Reijerse, *Chem. Rev.*, 2014, **114**, 4081–4148.
3 H. Dobbek, V. Svetlitchnyi, L. Gremer, R. Huber and O. Meyer, *Science*, 2001, **293**, 1281–1285.
4 J.-H. Jeoung and H. Dobbek, *Science*, 2007, **318**, 1461–1464.
5 E. E. Benson, C. P. Kubiak, A. J. Sathrum and J. M. Smieja, *Chem. Soc. Rev.*, 2009, **38**, 89–99.
6 S. Hammes-Schiffer, *J. Am. Chem. Soc.*, 2015, **137**, 8860.
7 R. Francke, B. Schille and M. Roemelt, *Chem. Rev.*, 2018, **118**, 4631–4701.
8 E. Fujita, C. Creutz, N. Sutin and B. S. Brunschwig, *J. Am. Chem. Soc*, 1993, **32**, 2657–2662.
9 J. Schneider, H. Jia, K. Kobiro, D. E. Cabelli, J. T. Muckerman and E. Fujita, *Energy Environ. Sci.*, 2012, **5**, 9502–9510.
10 J. D. Froehlich and C. P. Kubiak, *Inorg. Chem*, 2012, **51**, 3932–3934.
11 C. Costentin, G. Passard, M. Robert and J.-M. Savéant, *Proc. Natl. Acad. Sci.*, 2014, **111**, 14990–14994.
12 I. Azcarate, C. Costentin, M. Robert and J.-M. Saveánt, *J. Am. Chem. Soc.*, 2016, **138**, 16639–16644.
13 E. M. Nichols, J. S. Derrick, S. K. Nistanaki, P. T. Smith and C. J. Chang, *Chem. Sci.*, 2018, **9**, 2952–2960.
14 A. Chapovetsky, T. H. Do, R. Haiges, M. K. Takase and S. C. Marinescu, *J. Am. Chem. Soc.*, 2016, **138**, 5765–5768.
15 A. Chapovetsky, M. Welborn, J. M. Luna, R. Haiges, T. F. Miller III and S. C. Marinescu, *ACS Cent. Sci.*, 2018, **4**, 397–404.
16 J. Hawecker, J.-M. Lehn and R. Ziessel, *J. Chem. Soc. Chem. Commun.*, 1984, **984**, 328–330.
17 J. Hawecker, J.-M. Lehn and R. Ziessel, *Helv. Chim. Acta*, 1986, **69**, 1990–2012.
18 M. Stanbury, J.-D. Compain and S. Chardon-Noblat, *Coord. Chem. Rev.*, 2018, **361**, 120–137.
19 K. A. Grice and C. P. Kubiak, *Adv. Inorg. Chem.*, 2014, **66**, 163–188.
20 J. Agarwal, T. W. Shaw, H. F. Schaefer and A. B. Bocarsly, *Inorg. Chem.*, 2015, **54**, 5285–5294.
21 K. T. Ngo, M. Mckinnon, B. Mahanti, R. Narayanan, D. C. Grills, M. Z. Ertem and J. Rochford, *J. Am. Chem. Soc*, 2017, **139**, 2604–2618.
22 S. Sung, X. Li, L. M. Wolf, J. R. Meeder, N. S. Bhuvanesh, K. A. Grice, J. A. Panetier and M. Nippe, *J. Am. Chem. Soc*, 2019, **141**, 6569–6582.
23 D. A. Popov, J. M. Luna, N. M. Orchanian, R. Haiges, C. A. Downes and S. C. Marinescu, *Dalt. Trans.*, 2018, **47**, 17450–17460.
24 S. A. Chabolla, C. W. Machan, J. Yin, E. A. Dellamary, S. Sahu, N. C. Gianneschi, M. K. Gilson, F. A. Tezcan and C. P. Kubiak, *Faraday Discuss.*, 2017, **198**, 279–300.
25 L. Rotundo, C. Garino, E. Priola, D. Sassone, H. Rao, B. Ma, M. Robert, J. Fiedler, R. Gobetto and C. Nervi, *Organometallics*, 2019, **38**, 1351–1360.
26 J. Willkomm, E. Bertin, M. Atwa, J.-B. Lin, V. Birss and W. E. Piers, *ACS Appl. Energy Mater.*, 2019, **2**, 2414–2418.
27 S. Sung, D. Kumar, M. Gil-Sepulcre and M. Nippe, *J. Am. Chem. Soc*, 2017, **139**, 13993–13996.
28 P. Kurz, B. Probst, B. Spingler and R. Alberto, *Eur. J. Inorg. Chem.*, 2006, **2006**, 2966–2974.
29 F. P. A. Johnson, M. W. George, F. Hartl and J. J. Turner, *Organometallics*, 1996, **15**, 3374–3387.
30 M. L. Clark, L. Cheung, M. Lessio, E. A. Carter and C. P. Kubiak, *ACS Catal.*, 2018, **8**, 2021–2029.
31 B. P. Sullivan, C. M. Bolinger, D. Conrad, W. J. Vining and T. J. Meyer, *Chem. Commun.*, 1985, **6**, 1414–1416.
32 C. W. Machan, S. A. Chabolla, J. Yin, M. K. Gilson, F. A. Tezcan and C. P. Kubiak, *J. Am. Chem. Soc.*, 2014, **136**, 14598–14607.
33 D. J. Martin, B. D. Mccarthy, E. S. Rountree and J. L. Dempsey, *Dalt. Trans.*, 2016, **45**, 9970–9976.
34 C. Costentin and J.-M. Saveánt, *ACS Catal.*, 2018, **8**, 5286–5297.